Journal of Power Sources 195 (2010) 118–123

Contents lists available at ScienceDirect

Journal of Power Sources

journal homepage: www.elsevier.com/locate/jpowsour

# LSCF–SDC core–shell high-performance durable composite cathode

Seungho Lee [a], Hwa Seob Song [a], Sang Hoon Hyun [a], Joosun Kim [b], Jooho Moon [a,*]

[a] Department of Materials Science and Engineering, Yonsei University, 134 Shinchon-dong Seodaemun-gu, Seoul 120-749, Republic of Korea
[b] Center for Energy Materials Research, Korea Institute of Science and Technology, Seoul 136-791, Republic of Korea

ARTICLE INFO

*Article history:*
Received 15 April 2009
Received in revised form 22 May 2009
Accepted 8 June 2009
Available online 2 July 2009

*Keywords:*
Cathode
Durability
Composite
Core–shell particles
Solid oxide fuel cell

ABSTRACT

Core–shell type $La_{0.6}Sr_{0.4}Co_{0.2}Fe_{0.8}O_{3-d}$ (LSCF)–$Sm_{0.2}Ce_{0.8}O_{2-d}$ (SDC) powders are synthesized to achieve a high-performance durable cathode for intermediate temperature solid oxide fuel cells (IT-SOFCs). The SDC core size is controlled so that all core particles are surrounded by the LSCF particles with no unattached spots. Such a core–shell composite cathode develops an ideal microstructure with improved phase contiguity, homogeneity, and maximized triple-phase boundary density. The cathode that involves an SDC core of 500 nm exhibits the lowest interfacial polarization resistance (0.265 $\Omega\,cm^2$ at 650 °C), as well as long-term stability during both thermo-cyclic and electrochemically accelerated tests.



## 1. Introduction

Recently, there has been considerable interest in lowering the operation temperature of solid oxide fuel cells (SOFCs). Operating SOFCs at intermediate temperature (IT) (500–700 °C) not only prolong the lifetime of fuel cell stack components, but also allow the use of low-cost interconnect and balance-of-plant materials [1,2]. Unfortunately, commonly used cathode materials (e.g., $La_{0.7}Sr_{0.3}MnO_{3-d}$ (LSM)) lose their electrocatalytic activity at intermediate/low temperatures so that the cathodic interfacial polarization resistance becomes predominant over the anodic polarization resistance and the ohmic resistance. Hence, the development of a novel and high-performance cathode is essential.

Mixed ionic and electronic conductors (MIECs) such as $La_{0.6}Sr_{0.4}Co_{0.2}Fe_{0.8}O_{3-d}$ (LSCF), $Sm_{0.5}Sr_{0.5}Co_{0.5}O_{3-d}$ (SSC) and $Ba_{0.5}Sr_{0.5}Co_{0.2}Fe_{0.8}O_{3-d}$ (BSCF) have been extensively investigated as cathode materials for IT-SOFCs [3–5]. Among these materials, LSCF possesses a thermal expansion coefficient (TEC) that is well-matched with both doped zirconia-based and ceria-based electrolyte materials. Moreover, most of the recent high-performance cathodes are utilized in the form of a composite by mixing with an ionically conducting phase, e.g., a composite of LSCF with samarium doped ceria (SDC) [6,7]. The improved performance results from an extension of the triple-phase boundary (TPB) from cathode-electrolyte interface to the whole cathode surface.

The starting particulate materials and processing conditions are important determinants of the performance and durability of the cathode [8,9]. The starting powders used to fabricate the composite cathode can be a simple micro-scale mixture of two phases or nano-scale composite powders in the form of either a surface coated or core–shell structure. Such nano-composite powders mixed on a much finer length scale yield cathodes with better long-term stability and high-performance. A highly durable cathode for high-temperature SOFCs has been developed by utilizing well-engineered LSM/YSZ nano-composite particles in which YSZ grain particles of relatively large size are coated with both YSZ and LSM nanoparticles [10,11]. In the present study, we used a similar approach to achieve a high-performance and durable cathode for IT-SOFCs. Special emphasis is focused on the synthesis of a core–shell type LSCF-SDC composite cathode, in which the LSCF surface phase is attached on the SDC core. The particle size of the SDC core is carefully controlled to optimize the microstructure, such as phase connectivity, pore size, and pore distribution, all of which interplay to determine the cathodic performance and durability.

## 2. Experimental

Core–shell type LSCF-SDC nano-composite cathode particles were prepared by the polymerizable complex method. The nitrate salts of La, Sr, Co, and Fe were dissolved in water at a molar ratio of 2.9:2:1:4 in an attempt to synthesize $La_{0.58}Sr_{0.4}Co_{0.2}\ Fe_{0.8}O_{3-\delta}$. Next, ethylene glycol and citric acid were added to bind the metal cations. After a polymerization reaction at 100 °C, the SDC core particles were suspended in a polymeric resin. SDC core particles of mean size ~130 nm (denoted *SDC013*), 500 nm (*SDC050*) and

* Corresponding author. Tel.: +82 2 2123 2855; fax: +82 2 365 5882.
*E-mail address:* jmoon@yonsei.ac.kr (J. Moon).

0378-7753/$ – see front matter © 2009 Elsevier B.V. All rights reserved.
doi:10.1016/j.jpowsour.2009.06.079

2 μm (*SDC200*) which had been separately synthesized by the polymerizable complex method were added to the resin to prepare the composite particles. When *SDC013* was utilized, the resulting LSCF-SDC core–shell (*CS*) particles were denoted as *CS013*. The resin mixture containing the core particles was pyrolyzed in air at 400 °C for 2 h to eliminate volatile species, followed by calcinations at 800 °C for 4 h. The procedure resulted in core–shell type composite particles. The particle size was analyzed by a laser scattering particle size analyzer (Nanotrac 150, Microtrac Inc. Montgomeryville, PA). The morphology of the particle was observed by high-resolution transmission electron microscopy (HRTEM, JEM-2100F, JEOL) and compositional mapping within the particles was obtained by energy dispersive X-ray spectroscopy (EDS).

The electrolyte-supported symmetric cathode|SDC|cathode cells were prepared using two different LSCF–SDC composites: core–shell type powders and simple mechanically mixed powders (*MM013*) between LSCF (mean particle size of 0.12 μm) and SDC (mean particle size of 0.13 μm). Both of the composite particles had the same overall composition of LSCF:SDC = 50:50 in weight%. A cathode layer was deposited on both sides of the SDC electrolyte disc (diameter of 25 mm and thickness of 0.5 mm, sintered at 1400 °C for 4 h) by screen-printing using paste materials that were a mixture of the powders and additives dispersed in an organic solvent, followed by firing at temperatures from 750 to 900 °C for 4 h. After sintering, a platinum mesh connected to a platinum wire was attached to the cathode layer for current-collection by means of platinum paste. The area of the applied cathode was 1.5 $cm^2$ and the thickness was about 10 μm. The cross-sectional microstructures of the resulting composite cathodes were investigated by means of using scanning electron microscopy (FE-SEM, JSM 6700F, JEOL). The mercury intrusion method (Autopore IV, Micrometritics) was used to characterize the porosity and pore size of each cathode.

Electrochemical impedance measurements were performed in symmetrical cells using a.c. impedance spectroscopy (Solartron SI 1260/1287). The impedance spectra were obtained in the frequency range of 100 kHz to 0.1 Hz with an applied a.c. voltage amplitude of 20 mV at 650 °C. A pyramid-type cyclic current load was used for accelerated life-time tests (ALTs). Each load consisted of a cyclic current load, in which the current was applied from 0.2 to 1 A $cm^{-2}$ for the half-cell test. Each cyclic period lasted 30 min.

## 3. Results and discussion

HRTEM images of the synthesized core–shell nano-composite particles, in which an SDC core of ~130 nm was used, are shown in Fig. 1. The compositional mapping detected by EDX enables a distinction to be made between the LSCF and SDC phases. Composite particles can be divided into two different regions: SDC-rich regions (darker area) and SDC-deficient regions (brighter area). Detailed composition profiles obtained from selected areas in the TEM image are summarized in Table 1. Spectrum 1 originated from the bright area corresponds to the LSCF phase coated on the SDC core, whereas the darker phase is recognized as the SDC core with a diameter of 110–130 nm based on spectra 2 and 3. The La and Fe elements are distributed uniformly on the agglomerated composite particles, while the Sm and Ce elements are segregated in the dark middle region. EDX compositional mapping clearly confirms that the polymeric resin method effectively produces core–shell type, multicomponent, composite particles via uniform coating of the SDC core with LSCF. It should be noted that the core–shell particles have distinct morphological features compared to the mechanically mixed composite particles in which LSCF and SDC are simply mixed on a much larger length scale (the result is not shown here). Such a morphological difference in the starting particles can, in turn, influence variations in cathodic performance.

**Table 1**
Composition distribution (atomic %) of synthesized core–shell composite particle determined by energy dispersive X-ray (EDX) spectroscopy.

| Region | La | Sr | Co | Fe | Ce | Sm |
|---|---|---|---|---|---|---|
| Spectrum 1 | 0 | 18.51 | 5.09 | 24.91 | 3.28 | 4.43 |
| Spectrum 2 | 8.21 | 5.16 | 0.90 | 4.86 | 65.37 | 15.50 |
| Spectrum 3 | 7.72 | 1.69 | 1.00 | 3.33 | 72.31 | 13.96 |

Fig. 2 shows the variations of the interfacial polarization resistances ($R_p$) during the ALTs at 650 °C for composite cathodes prepared from two different core–shell particles (*CS013* and *CS050*) and the mechanically mixed particles (*MM013*). The initial $R_p$ values for cells with *MM013*, *CS013* and *CS050* are 0.615, 0.53 and 0.265 Ω $cm^2$, respectively. The $R_p$ corresponding to the core–shell cathodes is lower than that of the mechanically mixed cathode. Cathodic polarization resistance is determined by TPB site density and ionic/electronic conductivities. The lower $R_p$ associated with core–shell cathodes is due to a larger TPB site density and well-established ionic and electronic pathways, that arise from better homogeneous mixing at the nanometer length scale. Moreover, the $R_p$ value for *CS050* remains almost unchanged, even after 120 h of cyclic stress, whereas the $R_p$ values for *MM013* and *CS050* increase by 146 and 131%, respectively, after a 60 h cyclic test. In particular, the marked increase in the *MM013* cathode can be attributed to

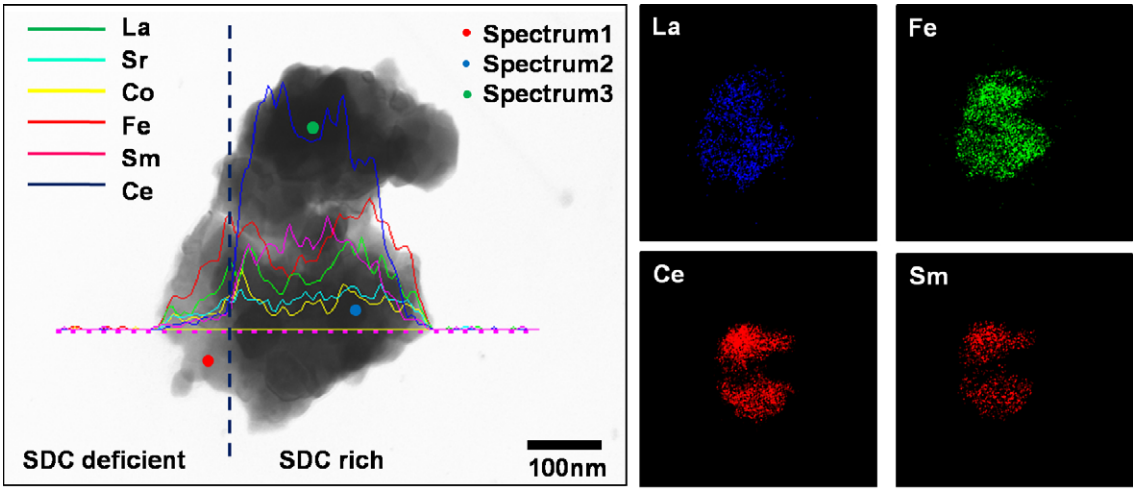


**Fig. 1.** HRTEM and corresponding compositional mapping of synthesized core–shell LSCF/SDC composite powders.

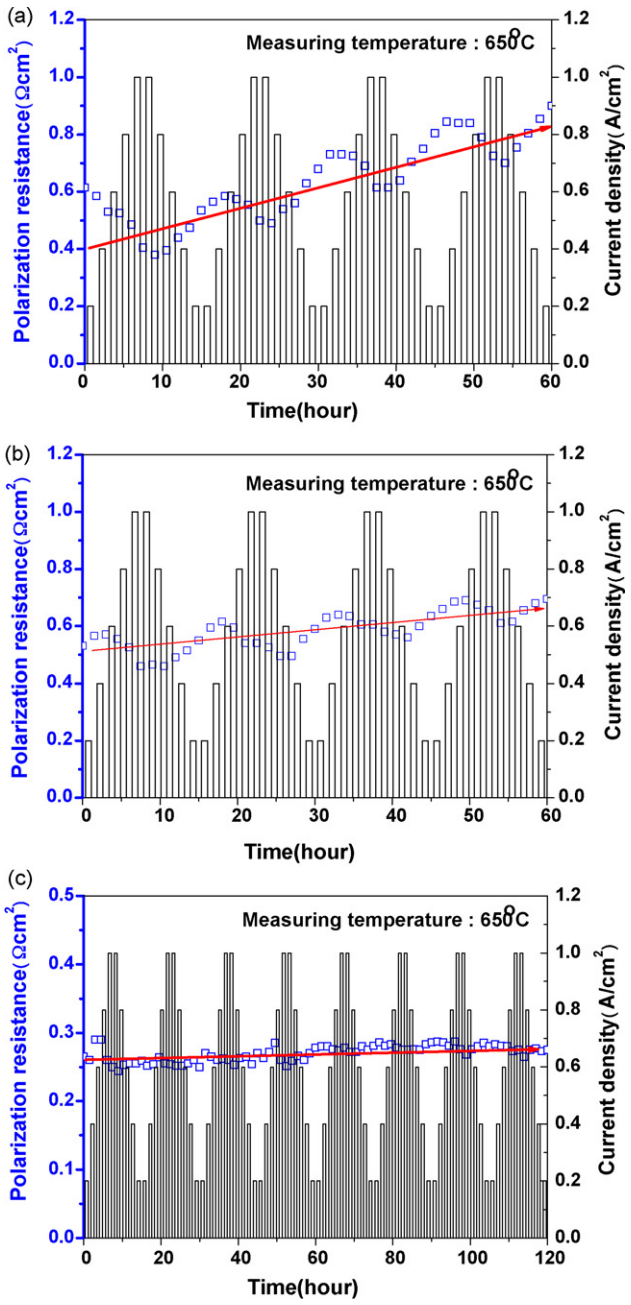


**Fig. 2.** Variation of interfacial polarization resistance for various composite cathodes during ALTs at 650 °C: (a) *MM013*, (b) *CS013*, and (c) *CS050*.

a reduction of TPB sites, possibly due to thermally and/or electrochemically driven coarsening of the less-stable LSCF phase.

When the core–shell type particles are used as a starting material, the SDC core size and the sintering temperature significantly influence the microstructure of the cathode. The cathodic performance as a function of sintering temperature and SDC core size is presented in Fig. 3. The optimum sintering temperature where $R_p$ is minimized differs depending upon the SDC core size. The optimum sintering temperature for the *CS013* and *CS050* cathodes is 850 °C, whereas $R_p$ reaches a minimum when the *CS200* cathode is sintered at 800 °C. This observation indicates that the SDC core size influences the sintering behaviour of the cathode and, in turn, determines the cathodic performance. The *CS050* cathode in which the SDC core belongs to the medium size range gives the best performance (0.265 Ω cm$^2$ at 650 °C) when sintered at 850 °C.

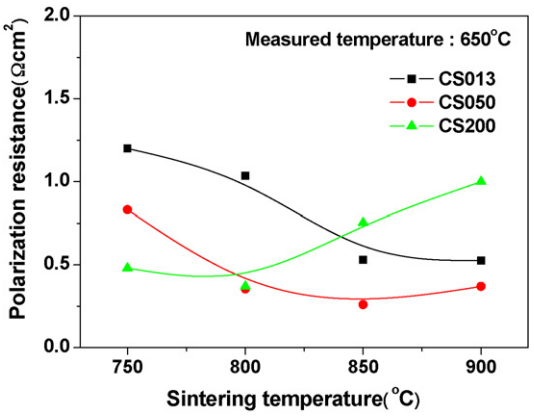


**Fig. 3.** Cathode polarization resistance of symmetric cell (core–shell cathode/SDC/core–shell cathode) as function of sintering temperature and SDC core size.

Impedance spectra analysis as a function of oxygen partial pressure can provide useful information regarding the cathodic performance with respect to its microstructure features. It has been reported [12,13] that the impedance spectrum of a composite cathode can be divided into two different arcs denoted *resistance A* ($R_A$ at high frequency) and *resistance B* ($R_B$ at low-frequency), each of which represents a dominant electrode kinetic process. *Resistance A* can be influenced by the transport of oxygen ions through the LSCF-SDC cathode. In other words, the magnitude of $R_A$ relates to the phase interconnectivity between the SDC powders. *Resistance B*, which is characterized by a strong oxygen pressure dependence, is presumably associated with the charge-transfer process that occurs at the reaction site. Thus, $R_B$ mainly reflects electrochemical oxygen reduction on the cathode, which is a strong function of the reaction site density.

In order to separate arcs of cathode impedance into $R_A$ and $R_B$, the *CS013* cathode was evaluated at 650 °C as a function of oxygen partial pressure ($P_{O_2}$), as illustrated in Fig. 4a. Jensen et al. [14] suggested the use of a difference plot in which the difference in the derivative of the spectrum with respect to the frequency ($f$) obtained between a specific and reference oxygen partial pressures (i.e., $\Delta\left(\partial Z_{real}/\partial \log f\right) = [(\partial Z_{real}^{0.21\,\mathrm{atm}\,P_{O_2}}/\partial \log f) - (\partial Z_{real}^{1\,\mathrm{atm}\,P_{O_2}}/\partial \log f)]$) is plotted against $\log f$ [14,15]. Such a graphical representation allows determination of the frequency at which the resistance variation is the most marked between two oxygen partial pressure conditions, as shown in Fig. 4b. The relative difference in the derivative of the resistance changes from a positive deviation to a negative deviation at $f$ = 50.1 Hz, and it reaches the maximum value at 3.2–12.6 Hz with increasing sintering temperature, which is characterized by a summit frequency ($f^{SUM}$) for the *resistance B* arc in the low-frequency region. The summit frequency for the *resistance A* arc in the high-frequency region is determined to be ~126 Hz using an equivalent circuit model. The fitted spectrum which is composed of two separated arcs located at the low and high summit frequencies, is well-matched with the experimentally obtained spectrum for the cathode (the red line in Fig. 4a). This demonstrates that it is possible to understand the sintering temperature induced variations of the electrode polarization by impedance analysis.

The resolved $R_A$ and $R_B$ polarization resistances as a function of sintering temperature and SDC core size are shown in Fig. 5. $R_B$ is predominant over $R_A$ so that the variation of the $R_B$ (Fig. 5b) is similar to that of $R_p$ (Fig. 3). The $R_A$ value gradually decreases with increasing sintering temperature, regardless of the SDC core size. This means that the ionic pathway in the cathode build up as the SDC phase undergoes sintering, as depicted in Fig. 5a. The *CS013*

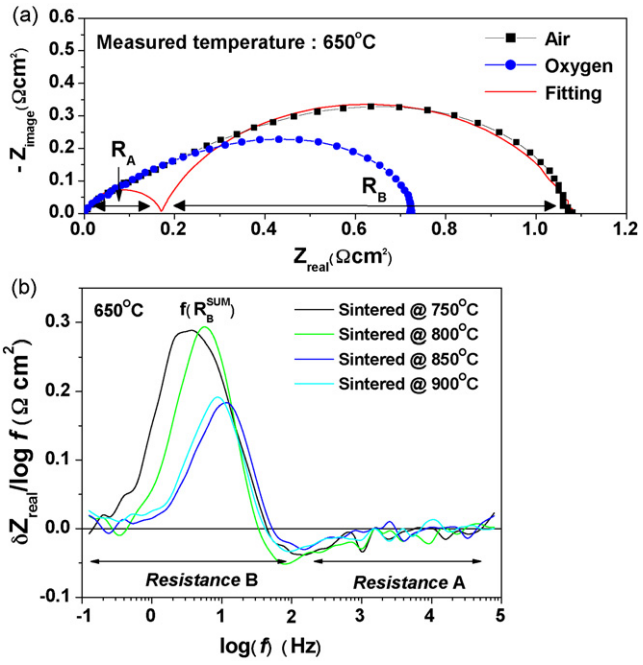


**Fig. 4.** (a) Nyquist plot for *CS013* cathode sintered at 850 °C measured in both air (squares) and oxygen (circles). Deconvoluted arcs are shown by dotted lines. (b) Difference plot of $\Delta\left(\partial Z_{real}/\partial \log f\right) = [(\partial Z_{real}^{0.21\,atm P_{O_2}}/\partial \log f) - (\partial Z_{real}^{1\,atm P_{O_2}}/\partial \log f)]$ against log*f*.

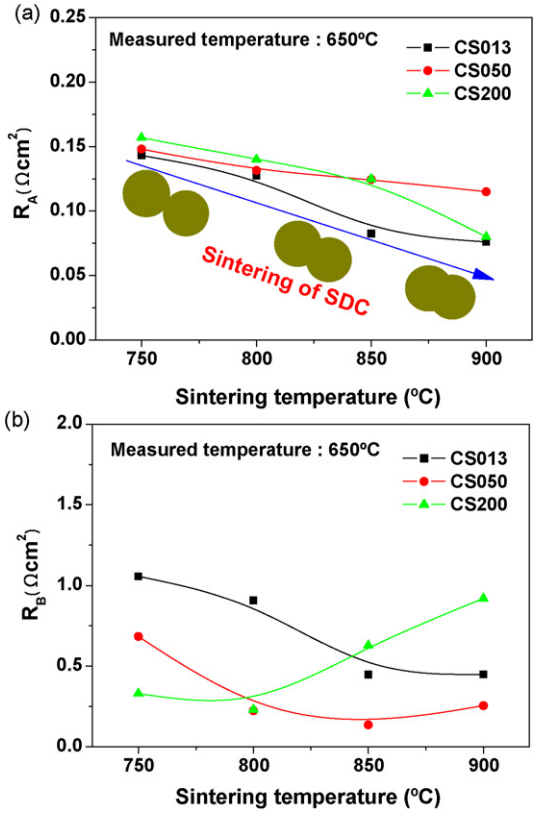


**Fig. 5.** Polarization resistance of process A ($R_A$) and process B ($R_B$) as function of sintering temperature. We obtained impedance spectra in obtained air using symmetrical cells deconvoluted into two arcs using $f_{R_A}^{SUM}$ and $f_{R_B}^{SUM}$ determined in Fig. 4a.

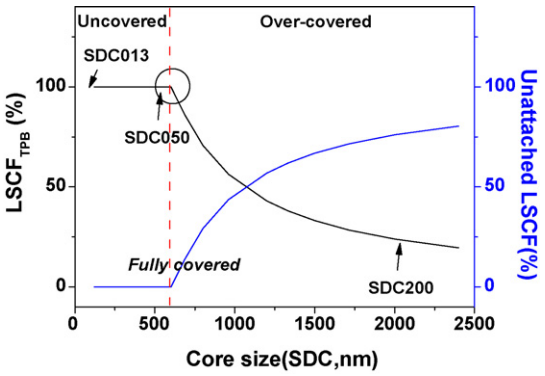


**Fig. 6.** Calculation of relative contribution of LSCF to form TPB in core–shell composite cathode as function of SDC core size.

and *CS200* cathodes experience a sharp decrease in $R_A$ as the sintering temperature increases, whereas a slight change is observed for the *CS050* cathode. This indicates that core–shell cathodes with either a fine or a large SDC core undergo significant densification at 850–900 °C.

Conversely, the sintering temperature dependence of $R_B$ varies significantly according to the SDC core size. The cathode with the smaller core (*SDC013*) exhibits relatively higher $R_B$ values than those with larger cores in the range of 750–900 °C, and it has a minimum resistance at 850 °C. By contrast, the cathode with a medium core (*SDC050*) shows relatively smaller $R_B$ values over the entire range of sintering temperature; the lowest value is reached at 850 °C. The cathode based on the larger core (*SDC200*) has lower resistance at the lower temperatures of 750–800 °C and the $R_B$ value soars when the sintering temperature increases from 800 to 900 °C.

In order to understand the relationship between the SDC core size and cathodic performance, a simple model is used to estimate the relative contribution of LSCF to form a TPB ($LCSF_{TPB}$) based on geometric consideration of the particle sizes. $LCSF_{TPB}$ can be defined as

$$LSCF_{TPB} = \frac{\text{Contact area of SDC/LSCF}}{\text{Total surface area of LSCF}}$$

based on the following assumptions: (i) spherical LSCF particles are uniformly surround the SDC core in a close-packed structure, (ii) the thickness of LSCF coating layer is equal to the diameter of the LSCF sphere, (iii) the contact area between each LSCF particle and SDC core is identical, which determines TPB length even when sintered. The variation of $LCSF_{TPB}$ as a function of the SDC core size at given LSCF particle size (120 nm) and LSCF:SDC = 50:50 in weight ratio is presented in Fig. 6. When the SDC is completely covered by all LSCF particles, the $LCSF_{TPB}$ reaches 100%, which is the case when the core size is ~600 nm. For cores below 600 nm, the $LCSF_{TPB}$ still maintains 100%, but bare spots exist on the SDC surfaces where the LCSF phase is unattached. These bare SDC core particles are sintered together without connecting with the LSCF phase, and sintering between the SDC core particles requires higher temperature. The *CS013* cathode sintered at 900 °C has a dense microstructure (porosity = 30%) with a small mean pore size (146 nm), as shown in Table 2. It is thought that the use of the smaller core leads to the formation of a dense

**Table 2**
Porosity and mean pore-size of core–shell composite cathodes sintered at 850 and 900 °C.

| Sintering temperature (°C) | 850 | | | 900 | | |
|---|---|---|---|---|---|---|
| Cathode | *CS013* | *CS050* | *CS200* | *CS013* | *CS050* | *CS200* |
| Porosity (%) | 55.9 | 63.1 | 62.4 | 30.4 | 59.8 | 49.9 |
| $D_{50}$ (nm) | 179.7 | 227.3 | 456.2 | 145.8 | 185.7 | 417.6 |

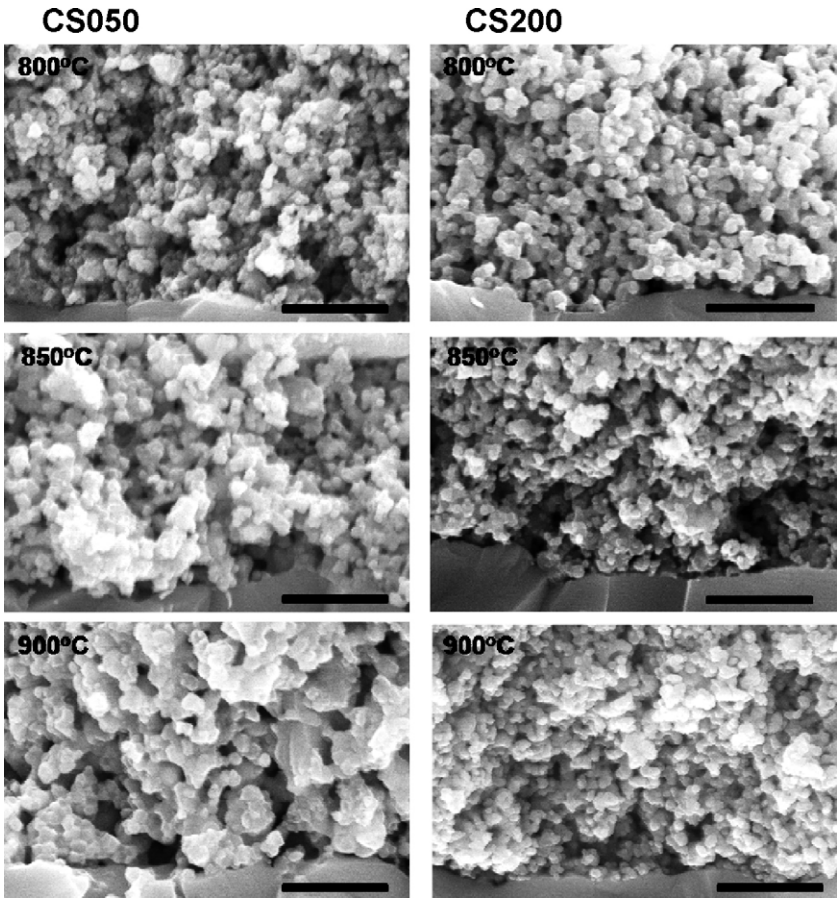


**Fig. 7.** SEM images of core–shell cathodes of *CS050* and *CS200* sintered between 800 and 900 °C. Scale bars represent 1 μm.

cathode structure that prevents a sufficient supply of oxygen to the TPB reaction site, thereby exhibiting the large $R_B$ value as shown in Fig. 5b. The dense cathode probably undergoes further densification during the ALT, which deteriorates the long-term stability, as shown in Fig. 2.

As the core size becomes larger than 600 nm, the amount of unattached LSCF phase gradually increases, and at the same time $LCSF_{TPB}$ declines. Such an unattached, less-stable LSCF phase would cause coarsening and phase segregation when exposed to high temperatures. The *CS200* cathode has an unattached LSCF of ~76%. This large quantity of unattached LSCF can densify the *CS200* cathode at relatively low temperatures (750–800 °C). The well-connected LSCF phase in the *CS200* cathode at 800 °C provides sufficient reaction sites for oxygen reduction, showing low $R_B$ value. The *CS200* cathode undergoes microstructural change, however, when subjected to high temperature sintering (850–900 °C) due to coarsening of the LSCF phase. This is characterized by a sharp increase in the $R_B$ value from 0.37 to 1 Ω cm$^2$, as shown in Fig. 5b [16]. The simple geomet-

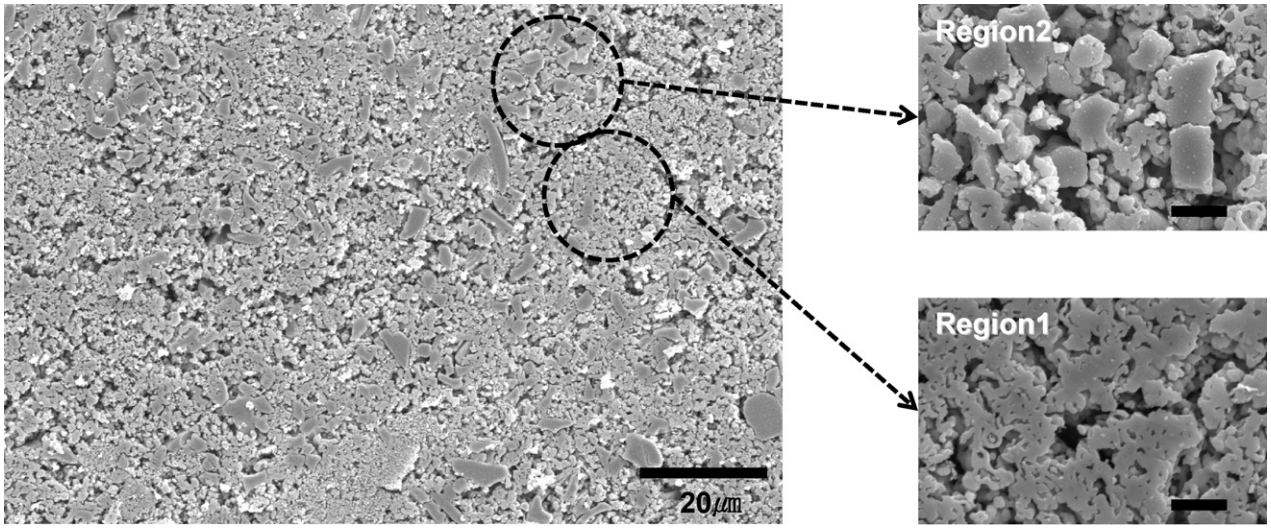


**Fig. 8.** SEM images of *CS200* cathode sintered at 900 °C and high magnification images for selected regions. Scale bar represents 2 μm.

**Table 3**
Local composition (atomic %) analysis by EDX for selected regions obtained from SEM image of core–shell cathode (*CS200*) in Fig. 8.

| Region | La | Sr | Co | Fe | Sm | Ce | O |
|---|---|---|---|---|---|---|---|
| 1 | 12.62 | 7.83 | 3.90 | 16.09 | 0 | 0 | 43.59 |
| 2 | 7.22 | 3.33 | 2.09 | 7.13 | 3.45 | 16.46 | 46.55 |

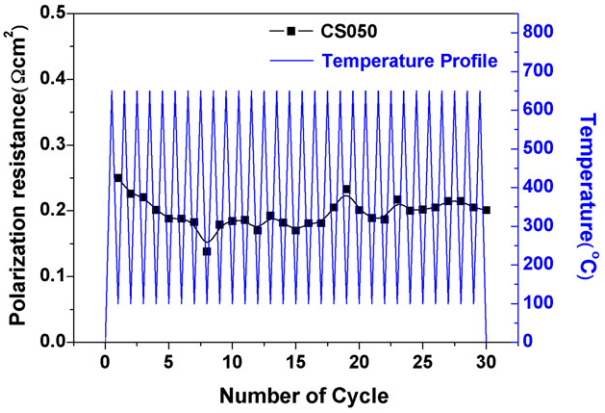


**Fig. 9.** Variation of interfacial polarization resistance of *CS050* cathode sintered at 850 °C during thermo-cyclic test performed between 100 and 650 °C.

rical calculation provides a clue as to why the core–shell cathode that utilizes the SDC core of 500 nm exhibits better electrochemical activity and long-term stability. For the *CS050*, it is concluded that the $LCSF_{TPB}$ reaches 100% and the SDC core surface is completely surrounded by LCSF. This proper attachment between the LSCF phase and the SDC phase leads to the formation of a well-interconnected composite microstructure with improved phase contiguity, homogeneity, and maximized TPB site density, which is manifested by the lowest $R_B$.

The cross-sectional microstructure of the *CS050* and *CS200* cathodes on the SDC electrolyte as a function of sintering temperature is shown in Fig. 7. There is no noticeable change in the microstructure of *CS050*, whereas the *CS200* becomes denser as the sintering temperature increases. Both samples have similar porosity (62–63%) when sintered at 850 °C, as shown in Table 2. By contrast, the porosities of the *CS050* and *CS200* cathode when sintered at 900 °C become 59 and 49%, respectively. According to the geometric model, the denser structure of the *CS200* that results from the sintering of the unattached LSCF phase, gives rise to the phase segregation. To confirm the microstructural homogeneity of the *CS200* composite cathode, the local structure and the composition were characterized by SEM and EDX, as shown in Fig. 8 and Table 3. The *CS200* composite cathode has a non-uniform microstructure segregated into two phases with different sized grain structures. One phase of larger grains ~2 μm (region 2) is determined to be a mixture of LSCF and SDC, while the other of smaller grains <0.5 μm (region 1) is composed of only LSCF. These segregated LSCF phases originate from the unattached LSCF, which causes the degradation of *CS200*.

The interfacial polarization resistance variation of the *CS050* composite cathode during the thermo-cyclic test is illustrated in Fig. 9. Furnace temperature periodically varies between 100 and 650 °C, as indicated in Fig. 9. During the thermo-cycle test, the polarization resistance remains nearly constant and even decreases slightly, possibly due to the thermal activation of the cathode microstructure [17]. Invariance of the polarization resistance during both the electrochemically accelerated lifetime test and the thermally accelerated cyclic test suggests that core–shell cathodes with proper sized cores show superior long-term thermochemical and electrochemical stability.

## 4. Conclusions

A core–shell type LSCF/SDC composite has been fabricated for the achievement of a high-performance durable cathode for IT-SOFCs. The relative size ratio between the SDC core and the LSCF shell particles plays an important role in determining the cathodic performance and the long-term stability. When the LSCF particles completely surround the SDC core with no unattached particles, the core–shell composite cathode develops an ideal microstructure with improved phase contiguity, homogeneity, and maximized TPB density. The use of a SDC core of 500 nm produces the lowest interfacial polarization resistance (0.265 Ω $cm^2$ at 650 °C). A composite cathode with a well-controlled microstructure maintains a nearly constant interfacial polarization resistance during both the 120 h electrochemically accelerated test and the 30-cycle thermo-cyclic test.

## Acknowledgements

This work is the outcome of the fostering project of the Specialized Graduate School of Hydrogen & Fuel Cells, that is financially supported by the Ministry of Commerce, Ministry of Knowledge Economy (MKE), Industry and Energy (MOCIE), and Seoul R&BD Program (CS070157). This study was also partially supported by the Korea Science and Engineering Foundation (KOSEF) through the National Research Lab Program funded by the Ministry of Education, Science and Technology (No. R0A-2005-000-10011-0).

## References

[1] B.C.H. Steele, A. Heinzel, Nature 414 (2001) 345–352.
[2] B.C.H. Steele, Solid State Ionics 134 (2000) 3–20.
[3] Y. Liu, W. Rauch, S. Zha, M. Liu, Solid State Ionics 166 (2004) 261–268.
[4] J.M. Serra, H.-P. Buchkremer, J. Power Sources 172 (2007) 768–774.
[5] Z.P. Shao, S.M. Haile, Nature 431 (2004) 170–173.
[6] C.J. Fu, K.N. Sun, N.Q. Zhang, X.B. Chen, D.R. Zhou, Electrochim. Acta 52 (2007) 4589–4594.
[7] E.P. Murray, M.J. Sever, S.A. Barnett, Solid State Ionics 148 (2002) 27–34.
[8] M.J. Jorgensen, S. Primdahl, C. Bagger, M. Mogensen, Solid State Ionics 139 (2001) 1–11.
[9] A. Hagiwara, N. Hobara, K. Takizawa, K. Sato, H. Abe, M. Naito, Solid State Ionics 178 (2007) 1123–1134.
[10] H.S. Song, S. Lee, S.H. Hyun, J. Kim, J. Moon, J. Power Sources 187 (2009) 25–31.
[11] H.S. Song, W.H. Kim, S.H. Hyun, J. Moon, J. Electroceram. 17 (2006) 759–764.
[12] M.J. Jorgensen, M. Mogensen, J. Electrochem. Soc. 148 (2001) A433–A442.
[13] M. Juhl, S. Primdahl, C. Manon, M. Mogensen, J. Power Sources 61 (1996) 173–181.
[14] S.H. Jensen, A. Hauch, P.V. Hendriksen, M. Mogensen, N. Bonanos, T. Jacobsen, J. Electrochem. Soc. 154 (2007) B1325–B1330.
[15] R. Barfod, M. Mogensen, T. Klemenso, A. Hagen, Y.-L. Liu, P.V. Hendriksen, J. Electrochem. Soc. 154 (2007) B371–B378.
[16] S. Lee, H.S. Song, S.H. Hyun, J. Kim, J. Moon, J. Power Sources 187 (2009) 74–79.
[17] Y. Sakito, A. Hirano, N. Imanishi, Y. Takeda, O. Yamamoto, Y. Liu, J. Power Sources 182 (2008) 476–481.